ELSEVIER

Deactivation of real three way catalysts by CePO$_4$ formation

C. Larese [a], F. Cabello Galisteo [a], M. López Granados [a,*], R. Mariscal [a],
J.L.G. Fierro [a], M. Furió [b], R. Fernández Ruiz [b]

[a] *Instituto de Catálisis y Petroleoquímica (CSIC), Cantoblanco, 28049 Madrid, Spain*
[b] *Servicio Interdepartamental de Investigación, Universidad Autónoma de Madrid,
Cantoblanco, Campus de la UAM, 28049 Madrid, Spain*

Abstract

The contaminants present in a real three way catalysts (TWC) aged under real working conditions for ca. 30 000 km have been determined. The X-ray fluorescence (TXRF) and energy-dispersive X-ray analysis (EDS) showed that P, Ca, Zn, Pb, Cr, Ni, Fe, Cd and Cu are present in the used catalysts. Distribution within the washcoat was scrutinised by scanning electron microscopy (SEM-EDS) analysis. The more external region (10–15 μm) of the washcoat are very concentrated in Ca and P. CePO$_4$ was detected by X-ray diffraction (XRD). Other phases that can be formed between contaminants themselves and with the washcoat components were not detected by XRD. Temperature-programmed reduction (TPR) experiments show that an important fraction of the Ce present in the washcoat is unable to participate in Ce^{3+}/Ce^{4+} redox pair under oxidising–reducing treatments. CePO$_4$ is proposed to explain the locking of the Ce^{3+}/Ce^{4+} redox couple. Although other contaminants like Pb can be also poisoning the catalyst, the formation of CePO$_4$ can be invoked to explain the worse catalytic properties displayed by used sample. The locked Ce pair is unable of participating in the rapid Ce^{3+}/Ce^{4+} redox couple required for correct oxygen storage capacity (OSC) properties and for the proper functioning of TWC.
© 2002 Elsevier Science B.V. All rights reserved.

Keywords: Deactivation; TWC; CePO$_4$

1. Introduction

Three way catalysts (TWC) have become the widely adopted solution of the car industry to fulfil legislation concerning the emission of more toxic components of the gas exhaust pipe of engine car. The installation of TWC in a catalyst cartridge at the exit of the spark ignition engine considerably reduces the concentration of NO$_x$, unburned hydrocarbon and CO [1–3]. Although TWC deteriorates under the tough conditions to which they are subjected (high temperatures and deposition of poisons) they have demonstrated their robustness to keep their efficiency after long time under running conditions (high mileage). However, the deactivation mechanisms is becoming a vivid topic of research [4–10] due to the fact that the legislation are becoming more stringent [11]. Consequently, the durability of the catalyst must be expanded if the increasingly low level of emissions must be fulfilled during the lifetime of the catalysts (more than 100 000 km). It is obvious that the understanding of the deactivation mechanisms is one of the key aspects in the achievement of more durable catalyst cartridges.

The deactivation by thermal effects are rather well known: sintering of active components results in a loss

of specific surface what it is clearly detrimental for the activity of the catalysts [7,8,12–14]. However, the role of chemical poisoning is less understood. It is well known that P, Ca, S, Pb and Zn are the most concentrated contaminants (P, Ca and Zn arising from lubricants and Pb and S from fuel) [5,6,9,15–20]. These studies must be updated and the information revisited because the nature and composition of the catalysts and the fuel are rapidly changing [11]. Moreover the phases that the contamination and the components of the catalyst built and the effect that these new phases have in the multiple functions the catalyst must operate are not well studied. This work is a contribution to the understanding of the role that P contamination has in the poisoning of the TWC. Real used catalyst extracted from the exhaust pipe of a gasoline car kindly supplied by Ford Spain with ca. 30 000 km was studied and characterised by several techniques especially fitted to this purpose. A fresh catalyst supplied also by Ford Spain with 0 km was used as a blank when required.

2. Experimental

2.1. Sample preparation

The catalytic container of a gasoline car usually carries two monoliths. The specimens were taken from the very beginning (first millimetres) of the upstream monolith of a Ford Focus 2.0 (1999 model) catalytic converter with 29 900 km. The samples studied in this work were small pieces separated from the monolith by breaking under gently pressure the honeycomb structure with a tweezers. The further treatment of the sample is critical for the characterisation of the sample: an optimal physical shape (pieces of monolith wall or powder obtained by grinding those pieces) must be selected according to the characterisation technique used and with the intention of improving the detection and stressing the chemical features that contamination brings about in the catalysts. Therefore, the physical shape will be clearly stated when describing the equipment for characterisation.

2.2. Characterisation techniques

TXRF analysis was performed in a Seifert EXTRA-II spectrometer (Rich Seifert & Co., Ahrensburg,

Germany), equipped with two X-ray fine focus lines, Mo and W anodes, and a Si(Li) detector with an active area of $80\,mm^2$ and a resolution of 157 eV at 5.9 keV (Mn Kα). To carry out the TXRF analysis X-ray tungsten source was used for P determination. The radiation was filtered with a Cu film of 10 μm thickness, in order to optimise the energy range (0–10 keV) used in the analysis. The X-ray molybdenum source was used for the analysis of the rest of elements, previously filtered with a Mo film of 50 μm. The exciting conditions used were a potential difference of 50 kV and a variable intensity—between 5 and 25 mA—to yield a count rate of about 5000 cps in the spectra acquired with the tungsten source and a potential difference of 50 kV and a variable intensity—between 5 and 30 mA—to yield a count rate of about 5000 cps in the spectra acquired with the molybdenum source. The analysed samples were subjected to the preparation process suggested [6,21] for the analysis of solid samples by TXRF [21–23]. First, 10 mg of a sample were ground to a powder of particle size less than 30 μm in an agate mortar. The powder was then further grounded for 20 min in a vibrating micro-pulveriser having a ball and a base of agate (Fritsch GmbH, Oberstein, Germany). Subsequently, 1 ml of high-purity water was added to the powder. Next, the mixture was poured into a test tube in which up to 2 ml high-purity water was added. The sample was homogenised for 10 min by ultrasonic desegregation in order to disperse possible agglomeration of particles. The 2 μl of the suspension was taken and placed on a flat carrier of plastic where the water was evaporated by vacuum. The errors (S.D.) was achieved with five replicates of the fresh and used samples.

The SEM-EDS analysis were obtained on an ISI-DS-130 scanning electron microscope coupled to a Si(II) X-ray detector and a Kevex 8000II processor for energy-dispersive X-ray analysis at 20 keV. The samples were pieces obtained by breaking the monolith in pieces with dimension in the range of millimeters. Two different studies were carried out. One type was intended to know the chemical composition of the outermost layer of the washcoat by placing the pieces in the sample holder with the washcoat exposed to the electrons beam (indicated as normal exposure in the Scheme 1 for the sake of simplicity, although an angle of ca. 30° between the normal
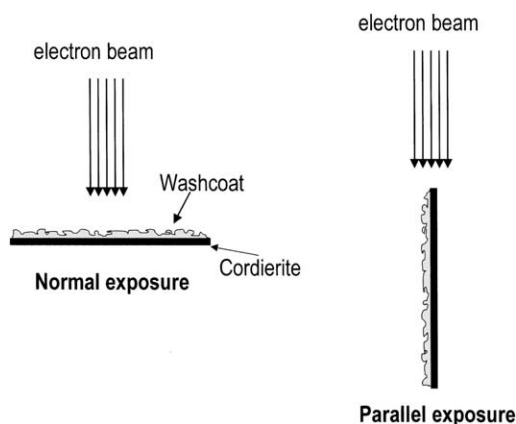
Scheme 1.

plane of the sample and electron beam exists). The electron probe was spotted at different regions in the washcoat (spot size ~1 μm diameter). The other type of studies were carried out in an attempt to obtain the profile of chemical composition within the washcoat by a line scan. To do so, pieces with the monolith wall cross sectioned were used. The pieces were placed in the sample holder as indicated in the Scheme 1 as parallel exposure. The line scan is the average of 10 consecutive individual line scans. The region where the line scan was carried out was selected by magnifying a region of the monolith wall ×1400. Line scan started at the cordierite and the other extreme of the line was placed at the outer part of the monolith wall.

Powder X-ray diffraction (XRD) patterns were recorded by scanning between 5 and 80° in the scan mode (0.02°, 2 s) by a Seiffert 3000 XRD diffractometer equipped with a PW goniometer with a Bragg–Brentano $\theta/2\theta$ geometry, an automatic slit and a bent graphite monochromator.

TPR profiles were recorded in a Micromeritics TPD/TPR 2900 equipment. The 100 mg of powder sieved between 0.60 and 0.80 mm and obtained by gently grinding the monolith walls were loaded in a U-shaped reactor. Before the TPR experiment, sample was calcined by heating the sample from ambient temperature to 773 K (heating rate 10 K/min) under a 3% O_2/He flow and kept at 773 K for 1 h. Then sample was cooled down to 313 K under this mixture and then switched to Ar and after 1 h switched to 10%

H_2/Ar mixture. When TCD signal of the equipment was constant, TPR profile was recorded by heating the sample from 313 to 1173 K at 5 K/min. Operating parameters like heating rate, sample loading, total flow rate and concentration of reducing agent were selected in such a way that the line profile, peak position and H_2 consumption could be determined accurately [24]. Quantification of the H_2 consumed in the reduction processes is accomplished through calibration of the equipment with reduction of CuO: different quantities of CuO were reduced and H_2 consumption during calibration were always close to the H_2 uptake detected in the TWC experiments.

2.3. Microactivity tests

Catalytic activity data were obtained by using a conventional fixed-bed plug flow reactor at atmospheric pressure. A gas mixture that intends to resemble the exhaust gas composition containing CO_2 (10 vol.%), H_2O (10 vol.%), NO (900 ppm), C_3H_6 (900 ppm), CO, H_2, O_2 and Ar (balance) was used. Mass flow controllers were used to feed the gases and a HPLC pump to feed the water. In an attempt to mimic the oscillation (frequency around 1 Hz) of the exhaust gas composition due to the close-loop control of A/F ratio, the concentration of (CO, H_2 and O_2) were cycled at 1 Hz oscillating at two different concentration values. These gases were cycled between 0.4 and 1.6 vol.% (CO); 0.13 and 0.53 vol.% (H_2), and 0.77 and 1.37 vol.% (O_2). These values define a central value for A/F = 14.63 and $\Delta\lambda = 0.03$ ($\lambda = $ (A/F)$_{actual}$/(A/F)$_{stoichiometric}$) according to formula described in [25]. The rapid selection between two different feedstreams was accomplished by fast valves electronically controlled following the same strategies described by González-Velasco et al. [7].

Gases were preheated and water pre-evaporated by cylindrical ovens set at 473 and 573 K, respectively, and placed upstream the catalytic bed. The catalyst bed consisted of 1 ml of particles between 0.6 and 0.8 mm resulting from gently crushing the monolith and mixtured and diluted in 2 ml of SiC (particle size 0.5 mm). Separation of the particles with different sizes was not detected. The catalytic activity was measured at 100 000 h^{-1} in light-off mode raising the temperature from 373 to 773 K at 3 K/min. Different detectors connected on line to the exit of

the reactor were used. NO was detected by chemi-luminiscence detector (HORIBA mod. CLA-510SS), CO and CO_2 by dispersive infrared detectors (Mod. HORIBA VIA-510), O_2 by paramagnetic detector (mod. HORIBA MPA-510) and C_3H_6, H_2 and H_2O by a quadrupole mass spectrometer (mod. BALTZER Prisma QMS 200 controlled by BALTZER Quadstar[TM] 422 software).

3. Results

Table 1 summarises the relative concentration of contaminants detected by TXRF with respect to Si (component of the cordierite) that was given the value of 100. Si, Al, Ce, Zr, Pd, Rh and other additives like Ba, well known components of the most efficient commercial catalysts [3,25], were detected in the fresh and used catalysts and not included in Table 1 for the sake of clarity. Si and Al are components of the cordierite ($5SiO_2·2Al_2O_3·2MgO$) used to shape the honeycomb monolith. Al (as Al_2O_3), Ce and Zr (as $Ce_{1-x}Zr_xO_2$ mixed oxide), and Pd and Rh are components of the washcoat where the active components are located [3,25]. Contaminants were considered those atoms present in the used sample that were absent or present in a much smaller concentration in the fresh sample. Most concentrated contaminants were P, Ca, Zn and Pb and other minor contaminants were Ni, Cr, Cd, and Cu. It is well known that Fe can be a minor component of the cordierite and thus the TXRF analysis cannot give a clear conclusion about Fe contamination that have been detected by other groups [19].

Table 1
Results of the TXRF characterisation of fresh and used samples

Element	Fresh	Used
Si	100 ± 1	100 ± 1
P	0.15 ± 0.03	3.9 ± 0.7
Ca	0.71 ± 0.05	1.09 ± 0.08
Zn	0.093 ± 0.001	0.41 ± 0.01
Pb	0.034 ± 0.001	0.42 ± 0.02
Cr	0.10 ± 0.01	0.17 ± 0.02
Cd	n.d.	0.17 ± 0.02
Cu	0.041 ± 0.002	0.091 ± 0.004
Ni	0.020 ± 0.002	0.05 ± 0.01
Fe	1.98 ± 0.04	1.57 ± 0.03

n.d.: not detected. Values are mass referred to Si = 100.

Additives of the lubricating oil, burned in the combustion chamber of the engine, originate compounds that reach the exhaust pipe and deposit P, Ca and Zn in the catalyst [5,16,18,26,27]. Pb originates from the Pb containing additives of gasoline [15,18,20,26,27], that are still present in gasoline although much more diluted than previous formulation gasolines. Ni, Cr, Cd and Cu arise from the metallic part of the engine as a consequence of the tough conditions the engine is subjected to during functioning [15,19].

In an attempt to locate the contaminant within the washcoat, SEM-EDS studies were carried out. Small pieces (few millimeters) laying on the sample holder by exposing the washcoat directly to the electron beams as described in Scheme 1 as normal exposure. Fig. 1 shows the EDS spectrum of both fresh and used samples, assignation of the lines are included in the figure. For the sake of clarity, the figure in the inset compares both spectra in the 1–6 keV zone. Al, Zr, Ce, Ba and Pd are again clearly identified in the washcoat of the fresh sample. The EDS spectrum of the used sample presents noticeable differences when compared to that of fresh catalyst. Very intense P and Ca lines are clearly detected and actually they are the most intense lines of the used spectrum. P and Ca are well identified contaminants of TWC catalysts that have been subjected to driving conditions: real ageing processes [16,19]. The signal of the washcoat components (Al, Zr, Ce, Ba and Pd) are clearly diluted by the P and Ca contamination that evidences the high level of contamination of these elements in the external region of the washcoat. It is important to stress that, although Zr L and P K lines can be superimposed due to their close energy position, the remarkable high concentration of P makes possible the assignation of the line at ca. 2 keV in the used sample to arise mainly from P contamination although the higher energy side of the peak must correspond to Zr emission. The inset of Fig. 1 where fresh and used spectra are compared and shows that Zr line position is slightly but patently shifted to higher energy in fresh sample. Other emission lines that could be assigned to other minor contaminants like Zn, Fe, Ni, Pb and Cu are slightly more intense that noise and quite close to EDS detection limit [28].

Fig. 2 presents the EDS analysis of carried out by randomly selecting another spot of washcoat. Ca is the more concentrated element in this zone of the
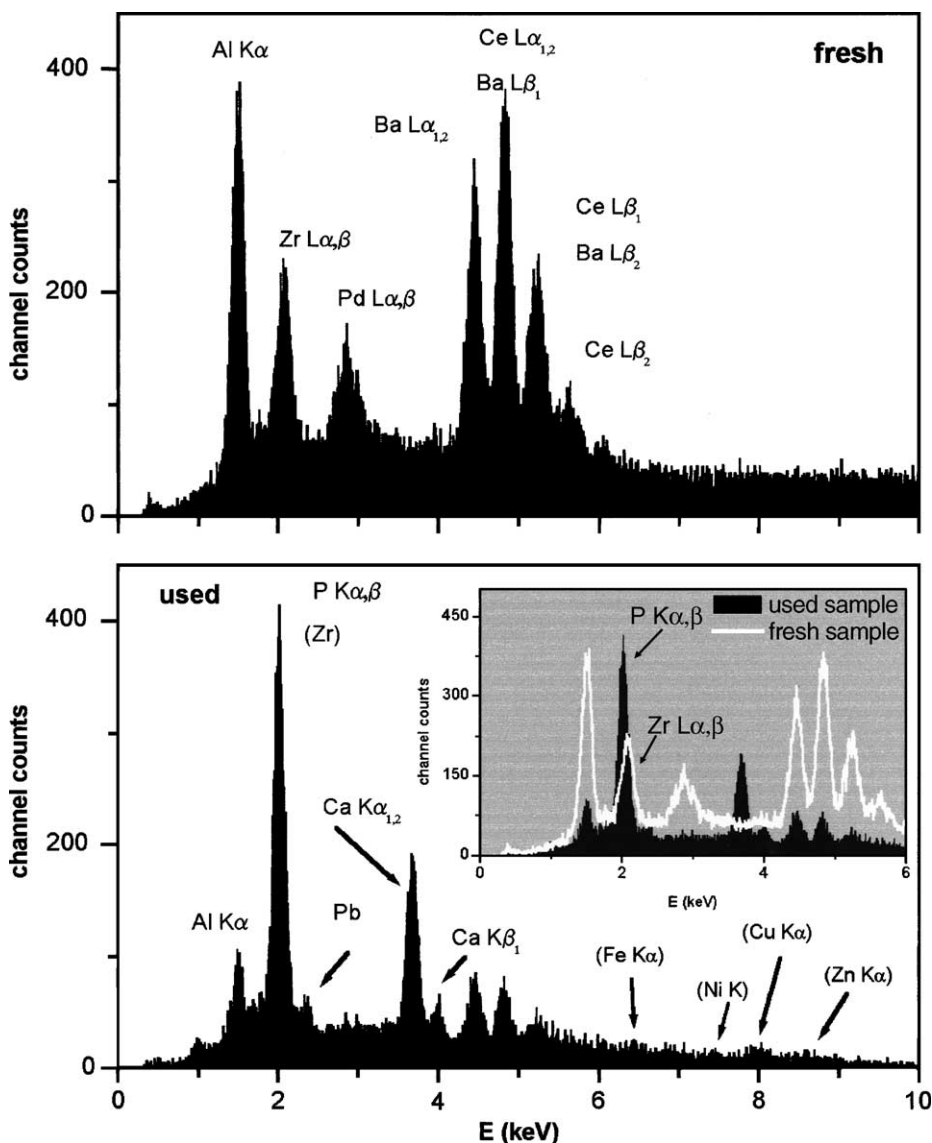
Fig. 1. EDS spectra of fresh and used samples. Inset is the same spectra but at different energy scale.

washcoat. The ratio between the intensity of the emission lines of Fig. 2 EDS spectrum are different to those of Fig. 1, which indicates that contamination is heterogeneously distributed in the washcoat at the micrometer scale. In Fig. 2 case, the signal from Fe, Ni and Zn contamination are more intense. The semiquantitative analysis obtained by applying ZAF correction to the EDS analysis of Fig. 2 are summarised in Table 2. The differences in the concentration found

when comparing results from TXRF and EDS analysis are due to the different procedure employed to prepare and analyse the samples. Fine powder obtained by thorough grinding in the case of TXRF analysis yields an average concentration. Intact pieces of the monolith wall in the case of the EDS analysis in normal exposure that provides a local information of the concentration in the upper most micrometers of the washcaoat. The lower level of Fe, Pb, Cu, Ni and Zn
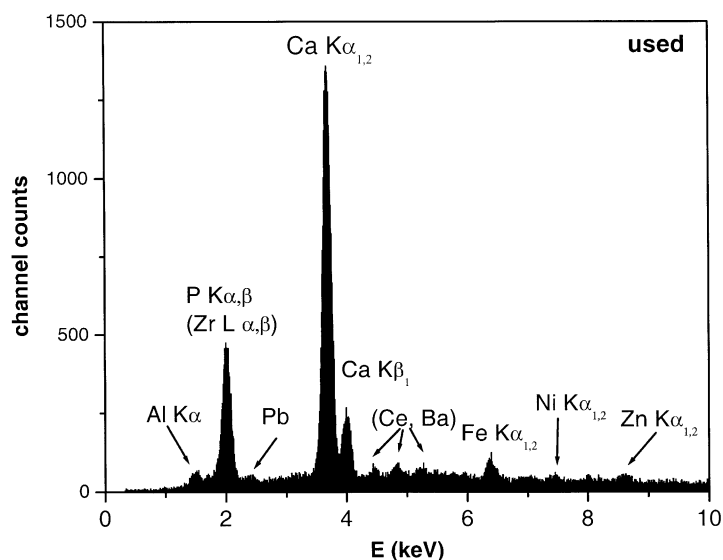
Fig. 2. EDS spectrum of used sample at a different spot that spectrum of used sample presented in Fig. 1.

contamination detected in the used catalysts, even in this spot where the contamination was comparatively high, agrees with the TXRF results.

The second aspect to be commented is that Si, a component of the cordierite, the major structural constituent of the ceramic monolith is not detected. The EDS technique supplies information of a few micrometers depth, washcoat in TWC has more

Table 2
Atomic percent of elements detected by SEM-EDS analysis in the fresh and used samples

Sample	Fresh	Used	Energy region for the line scan analysis (eV)
Al	52.0	2.1	1440–1534
Si	–	–	1692–1788
Ce	15.5	0.9	4774–4904
Zr	13.3	1.1	1963–2063[a]
Ba	16.2	1.9	4401–4528
Pd	3.0	0.1	2783–2893
P	n.d.	19.8	1963–2063[a]
Ca	n.d.	63.1	3631–3751
Zn	n.d.	3.9	
Fe	n.d.	4.5	
Ni	n.d.	1.4	
Cu	n.d.	1.2	

n.d.: not detected.
[a] The same region is selected for P and Zr detection.

than 15–20 μm. Therefore, the EDS signal from the cordierite and deep the washcoat are not detected by this configuration of the analysis. In an attempt to achieve a map of the approximate distribution of the contamination within the washcoat the EDS analysis was recorded by line scan methodology. The integration of the EDS signal within given energy regions of the EDS spectrum was carried out. Table 2 summarises the energy regions selected for the line scan analysis. Fig. 3 shows the line scan obtained in a fresh washcoat while Fig. 4 displays that of used catalysts. The cordierite–washcoat interphase detected in the line scan of the fresh catalyst is placed at around 10 μm from the beginning of the line scan (Fig. 3) as it can be derived from the parallel traces of the Si and Al signals between 0 and 10 μm (they even show very similar intensity what is consistent with the homogeneous composition of the cordierite) and the drastic decrease of the Si signal beyond this distance. On the other hand, Al trace is still clearly visible and even in some zones of the line scan is more intense than in the cordierite region because Al_2O_3 is a major component of the washcoat. The change in the intensity of the Al signal can be due to changes in the Al concentration within the washcoat. Line scan goes through different washcoat region where Al_2O_3 particles predominates over Ce–Zr mixed oxides
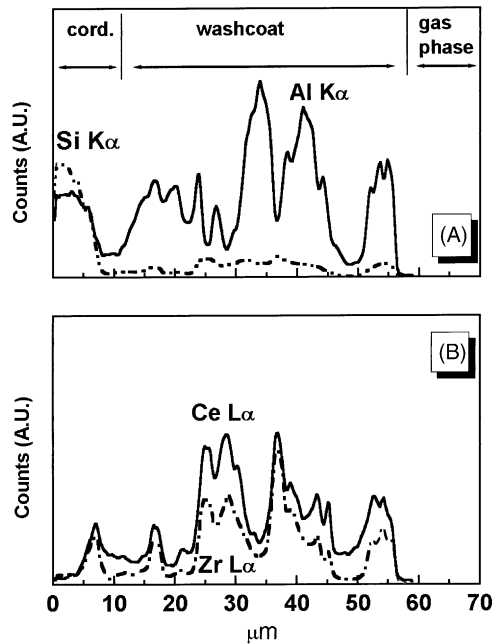
Fig. 3. Line scan traces on fresh sample: (A) Si and Al traces; (B) Ce and Zr traces.
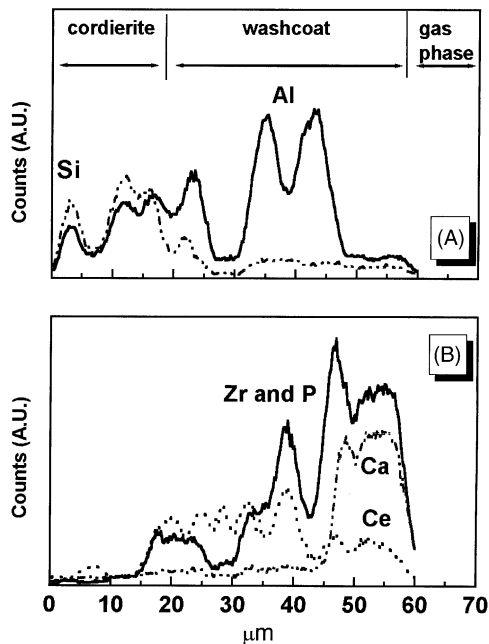

Fig. 4. Line scan traces on used sample: (A) Si and Al traces; (B) Ce, Ca and Zr(P) traces.

particles and Al signal becomes more intense than that of Ce and Zr. Obviously, the zone where Ce and Zr traces are more intense corresponds to grains of $Ce_{1-x}Zr_xO_2$ and the alumina becomes diluted by this mixed oxide. Moreover, it must be bear in mind that the porous nature of the washcoat (both intra- and interparticle) also contributes to changes in the intensity of the signal of the EDS probe (rough surface effects) [28].

In the fresh sample the Ce and Zr traces become clearly more intense after the cordierite–washcoat interface and obviously run parallels. In the used catalysts, a more complicated pattern is observed and very remarkable differences between the line profiles of the fresh and used catalysts can be found. The pulses collected in 1963–2063 eV region cannot be unequivocally assigned to either P or Zr due to the superposition of the Zr L and P K lines, and thus the signal between 1963 and 2063 eV and Ce traces does not run parallel throughout all the line scan. Actually, the 1963–2063 eV signal becomes very intense at the external side of the washcoat where the Ca signal also predominates. A remarkable decrease of the intensity of the Al and Ce signals is also detected at the external side of the washcoat. Both results indicates that the trace detected in the energy range between 1963 and 2063 eV at the external side of the washcoat must contain an important contribution due to the P. At the region of the washcoat closer to cordierite the trace must arise mainly from Zr. This strongly suggests that P and Ca contamination is mainly concentrated at the outer region of the washcoat closer to the gas phase. Similar results have been found in other studies carried out on modern TWC formulation [16] and on older Ce and Zr mixed oxides-free catalysts [15,17]. P and Ca arises from the lubricant additives that, when burned in the engine at high temperatures, are released to the exhaust gases as solid particles [27]. A diffusion controlled mechanism of deposition of particles containing P have been proposed to explain the concentration of the P contamination in the external side of the washcoat and a mathematical model have been successfully used to describe such deposition [29]. In any case, it is worthy to stress that the inner part of the washcoat close to the cordierite is clean or with low P–Ca contamination. In other words, there are regions where $Ce_{1-x}Zr_xO_2$ has been in contact with P contamination at high temperatures located at the
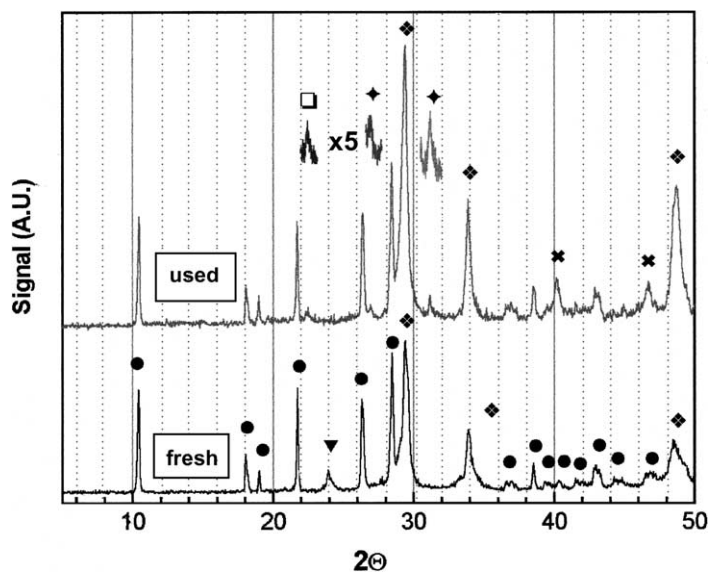
Fig. 5. XRD diffractograms of fresh and used samples.

outermost layer of the washcoat and zones free of P contamination (deep in the washcoat).

Fig. 5 displays the region $2\theta = 5$–50 of XRD diffractograms of fresh and used samples. The diffractogram of fresh sample presents reflections which can be clearly assigned to cordierite (reflections for cordierite are marked as ● in Fig. 5). Diffraction at $2\theta = 29.41$, 33.88 and 48.54 are assigned to $Ce_{1-x}Zr_xO_2$ mixed oxide (marked as ◈). The exact composition of the mixed oxide is beyond the scope of this study due to the commercial character of the sample. A Ce/Zr atomic ratio close to 1 was expected. Concerning the symmetry group of crystallisation, identification and assignation to any of the symmetry reported in literature (tetragonal symmetry (named t, t′ and t″) and a cubic phase (c) symmetry) [30] is complicated by the fact that cordierite also exhibits several reflections at angles close to the most intense peak of solid solution that makes wider the diffraction peaks and therefore imprecise the assignation. Although Raman spectroscopy (RS) and transmission electron microscopy (TEM) coupled with selected area electron diffraction (SAED) characterisation is required for a more precise assignation, this does not add relevant information to our work. Finally, the peak at 23.94 was assigned to tetragonal ZrO_2

(JCPDS file number 81-1329). The reference recalled by the file assigned this diffractogram to a tetragonal ZrO_2 stabilised by Ca. Other reflections from this phase were too weak to be detected or superimposed to other more intense reflections from cordierite.

The diffractogram of used catalyst displays several remarkable differences with respect to the fresh sample pattern. The most remarkable result is the detection of weak, but clearly visible, diffraction peaks at $2\theta = 26.96$ and 31.90 which were marked as ✦ in Fig. 5. A much more careful recording of the XRD pattern (0.005°/s, 5 s) was carried out with the aim to clarify the assignation and represented with a five times amplification in Fig. 5. These reflections were assigned, first to (2 0 0), and second to unresolved (0 1 2) and (−1 1 2) peaks of Ce(III) orthophosphate, $CePO_4$ (JCPDS file 83-0650). Other important $CePO_4$ reflections (like line at 28.80 corresponding to (1 2 0) plane) were obscured by diffraction lines of cordierite and of Ce–Zr mixed oxide.

Cordierite reflections are not altered but diffraction peaks of $Ce_{1-x}Zr_xO_2$ mixed oxide (marked as ◈) become narrower, more intense and clearly distinguished from the cordierite reflections. This effect can be explained by a sintering of the particles of the $Ce_{1-x}Zr_xO_2$ mixed oxide and agrees with other results

reported in bibliography both in laboratory samples and in real TWC [4,16,30]. The high temperatures reached by the catalyst monolith under running conditions justify the sintering of the Ce–Zr containing oxides of the washcoat. The most intense Pd diffraction lines (corresponding to (1 1 1) and (2 0 0) planes) were also visible (peaks at $2\theta = 40.12$ and 46.68, marked as ✖ in Fig. 5) (JCPDS file 46-1043) that also indicates sintering of the Pd particles due to the high temperatures underwent by the used catalyst.

The peak at $2\theta = 22.44$ (marked as ❑ in Fig. 5) could not be assigned to any phase. The complex composition of the commercial TWC makes difficult a definitive assignation. However, this peak cannot be due to any contamination because it was also detected in samples arising from downstream zones of the first monolith where contaminants concentrations are much smaller. Therefore, it must be related with sintering and improvements in the crystallisation of any of the unknown phases present in the catalysts. Any of the reported phases formed between contaminants and washcoat components like $AlPO_4$ phases, $MgZn_2(PO_4)_2$, $CaZn_2(PO_4)_2$, $Ca_3(PO_4)_2$, $Zn_3(PO_4)_2$ or $Zn_2P_2O_7$ [16,17,31] that have been detected by other groups in real used samples were not detected in our samples, possible Zr phosphates are also excluded. So these phases seems not be playing a role in the poisoning of the samples, or at least play a minor role.

Fig. 6 compares the TPR profile of fresh and used catalysts. The TPR profile of the fresh sample present at two peaks at low temperature (at ca. 353 and 378 K) and another wide and unresolved feature that stretches from 523 up to 1023 K. The assignations of the reduction features observed in the figure can be explained taking into consideration the conclusions of other groups that have studied the reduction of Pt group metals (PGMs) (like Pt, Pd and Rh) deposited on $(Al_2O_3$ supported) $Ce_{1-x}Zr_xO_2$ mixed oxides [32–34]. However, it must be bear in mind that a definitive assignation of the peaks is complicated by the commercial character of the samples that hinders the exact knowledge of the initial state of the sample. The first two peaks can be explained by the concomitant reduction of noble metals and of Ce^{4+} to Ce^{3+} located on the surface. The measurement of the H_2 consumed in these reduction peaks exceeded the amount needed for the reduction of the loading of noble metal present in the catalyst. H_2 spill-over from noble metal particles to Ce oxide has been explained to facilitate the reduction of surface Ce^{4+} [33,34]. The feature at higher temperature is more complex and several reduction processes seem to be involved. In principle, it could be assigned to reduction of the remaining bulk Ce^{4+}, although reduction of bulk Ce^{4+} has been reported to occur in fresh metal particles supported on Ce–Zr mixed oxides at higher temperatures [32–34]. The TPR profile of used sample displays large differences when compared to the fresh sample. Only one peak at low temperature (at 353 K) is now detected. Three more reduction processes occur at higher temperature (473, 633 and 973 K, respectively). Although additional characterisation is required for a more precise and true assignation, the attribution done for the fresh sample can be also applied for the used sample. The most notable result is that the amount of H_2 consumed in the TPR profile of the used sample is considerably smaller than that of the fresh sample: ca. 10 times lower for used sample. However, it must bear in mind that H_2 spillover phenomena can also involved in H_2 consumption. The former is not related with the creation of an O vacancy and the evolution of H_2O by reduction of Ce^{4+} oxide to Ce^{3+} oxide [35,36]. However, when TPR experiments involving fresh and used samples were carried out by analysing the composition of the gases at the reactor exit by mass spectrometry (TPR-MS), a much less intense H_2O formation was detected as well. Moreover, it must be stressed that very weak signals from CO_x evolution were detected
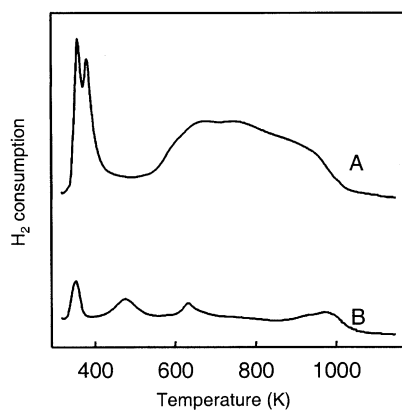

Fig. 6. TPR profiles after an oxidising pretreatment at 773 K of (A) fresh sample and (B) used sample.

when TPR experiments of fresh and used samples were carried out by analysing the composition of the gases by mass spectrometry (MS) connected on-line at the reactor exit. By no means CO_x (or NO_x) evolution can contribute to the reduction features detected by TCD equipment and showed in Fig. 6 as has been detected in the reduction of other Ce containing catalysts [37]. The intensity of the CO_x peaks detected by TPR-MS were two orders of magnitude less intense than reduction processes and NO_x evolution was not detected. The calcination step previous to the reduction experiment seems to have cleaned the surface of C and N containing adsorbates. Therefore, it can be said that the smaller amount of H_2 consumption in the TPR profile of the used sample is related with a lack of the amount of reducible Ce^{4+} oxide.

Other Ce^{3+} phases like $CeAlO_3$ or other intermetallic Ce-PGM were not detected by XRD in none of the samples studied in this work. $CeAlO_3$ has been observed in catalysts aged under real conditions which Zr was not present in the formulation. However, the formation of mixed $Ce_{1-x}Zr_xO_2$ oxides has been claimed to prevent the reaction between Ce^{3+} and Al_2O_3 to form $CeAlO_3$ [30]. Ce(III) is only detected in $CePO_4$. However, Ce should be as Ce^{4+} before the TPR experiment since fresh and used sample were previously calcined at 773 K. Chemical analysis showed that Ce, Pd and Rh concentrations in used sample are quite similar in both fresh and used samples Therefore, the remarkable decrease in the H_2 consumption detected in the used sample cannot be explained in terms of losses by attrition of reducible species during functioning in the exhaust pipe but for another reason. $CePO_4$ detected by XRD is expected to play a key role as it will be discussed below.

Fig. 7 shows the light-off curves obtained for the NO, CO and C_3H_6 conversion in fresh and used samples. The temperatures at which 50% of conversion of NO, CO and hydrocarbon (T_{50}) are attained is considerable higher (ca. 100 K) in used catalysts with respect to the fresh samples (even in the case of hydrocarbon conversion in used catalysts T_{50} cannot be reached). Moreover, the highest conversion that can be reached with the conditions utilised are clearly lower in the used catalysts. Both methods of describing the catalytic activity showed that the catalytic properties of the used sample are seriously damaged and presents much worse catalytic performance than fresh sample.
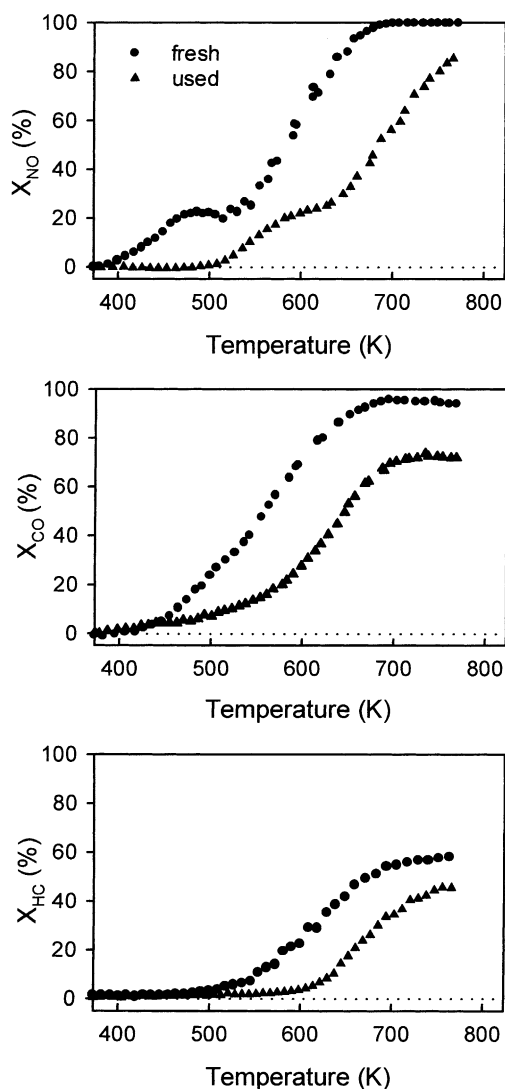

Fig. 7. NO, CO and C_3H_6 conversion on fresh (●) and used (▲) samples.

It is important to stress that it could be the case that the catalytic properties could remain intact especially in a real TWC with low mileage (30 000 km) like the one studied in this work.

4. Discussion

The detection of P, Ca, Zn, Pb, Fe, Ni, Cd, Cr and Cu contamination heterogeneously distributed

in the washcoat of the used catalyst shown in this work agrees with the results of other studies carried out by different groups on vehicle aged catalysts [15,16,19,26,27]. A very significant result presented in this work is the detection by XRD of $CePO_4$ (Ce(III) ortophosphate) reflections in the used sample. This phase has been recently detected by XRD in front portions of vehicle-aged catalyst with ca. 103 000 km [5]. Other authors have proposed that Ce phosphate is present in used TWC aged under real conditions although no direct evidence was presented [38]. Other authors have suggested that Ce(III) phosphates can be formed during real working conditions, $Ce(PO_3)_3$ *catena*-polyphosphate (metaphosphate) being the preferred assignation [16]. An indirect evidence was showed: this assignation was based on an increase of the ^{31}P signal from $AlPO_4$ when a used sample was calcined at high temperatures. This observation was interpreted as due to the formation of $AlPO_4$ at the expenses of Ce(III) phosphate: an inactive NMR phosphorous compound that reacts at high temperature with alumina to form $AlPO_4$. This latter result does not contradict the detection of ortophosphate. Sample of our study arise from a cartridge with 30 000 km instead of the much higher mileage vs. ca. 164 000 and 193 000 km presented by catalysts studied by Rokosz et al. [16] that can present a much higher P uptake and therefore Ce phosphates with higher P/Ce ratio are expected. It must be also taken into account the axial dependence of the uptake of contaminants. The concentration of contamination a few centimetres downstream the beginning of the monolith [15] is much lower than that at the frontmost region. Actually, it has been shown that beyond the first 8–10 mm the contamination is restricted to a layer few micrometers wide in the washcoat [39,40]. If the sample is not collected from the very first micrometer of the front monolith, any phase that can be formed between the contaminants and the washcoat components will be barely detected by XRD. Finally, it must be underlined that in the catalysts investigated in the above mentioned works Zr was not included in the formulation: Zr is an additive of more recent formulation of TWC catalysts. Therefore, our result indicates that Zr does not prevent the formation of $CePO_4$.

The finding of $CePO_4$ reflections demonstrates that a crystalline Ce(III) phosphate has been formed un-

der real working conditions. The presence of other amorphous Ce phosphates not XRD-visible cannot be discarded. The width and the low intensity of the peaks suggest that, although clearly visible, the sample is ill-crystallised. Moreover, the detection of $Ce_{1-x}Zr_xO_2$ mixed oxide in the used sample indicates that a great part of the Ce has not reacted with the P and still is as Ce–Zr oxide phase. The fact that Ca and Zn phases are not detected, although a crust containing Ca and P was evidenced by SEM-EDS, can be explained by considering the formation of impervious glassy Zn phosphate and a amorphous glaze-like Ca phosphate that has been described to be formed in used catalysts [16,17].

The relevance of the detection of $CePO_4$ in used TWC is related with the high thermal stability of Ce(III) valence state in Ce(III) phosphate. A number of research works have been devoted to study the conditions for the formation of Ce(III) or Ce(IV) phosphate and their stability at high temperatures [41,42]. Those studies show that the formation of a given Ce phosphate is strongly dependant on the starting P/Ce ratio and of the calcination temperature. Although several Ce(IV) phosphates have been described, Ce(IV) phosphates are unstable at high temperature (973–1073 K) and transformed to Ce(III) phosphates with O_2 evolution, even under O_2-rich conditions (like calcination under air). Moreover, other Ce phosphates slightly P-enriched have been described to decompose and transform to ortophosphate with O_2 evolution and P_2O_5 segregation [43]. All these data strongly suggest that $CePO_4$ is a very stable phase at high temperature even under O_2-rich atmosphere. Therefore, the detection of $CePO_4$ means that a detectable fraction of Ce atoms are as very stable Ce(III).

The remarkable depletion of the H_2 consumption observed in the TPR of used sample indicates that an important fraction of the Ce is unable to be oxidised in the previous calcination step that preceded the TPR recording and that the Ce^{3+}/Ce^{4+} pair is locking a great part of the Ce present in the sample. It is noticeable the fact that the small amount of $CePO_4$ detected by XRD can be locking so extensively the Ce^{3+}/Ce^{4+} pair. An explanation is that, although only a small amount of Ce is really locked as Ce^{3+} in $CePO_4$ phase, the Ce(III) phosphate is covering the Ce–Zr oxide particles. The Ce^{4+}/Ce^{3+} redox pair is still possible in the

underneath Ce–Zr mixed oxide but the Ce phosphate layer blocks and inhibits the reduction and reoxidation steps.

Excellent TWC performance under rich and poor O_2 oscillations in the composition of the exhaust gas is based on the buffering effect that the rapid Ce^{3+}/Ce^{4+} redox couple supplies (oxygen storage capacity, OSC). If the Ce^{3+}/Ce^{4+} couple is locked, the OSC is seriously damaged and so does the catalytic properties of the catalysts. Therefore, the rapid Ce^{3+}/Ce^{4+} pair that works properly in the fresh sample may be locked and unable to work efficiently in the used sample. This work has shown that a used catalyst with its catalytic performance seriously deteriorated also displayed the Ce^{3+}/Ce^{4+} pair locked. The worsening in the removal of C_3H_6, NO and CO detected in the catalytic activity of used sample cannot only be assigned to the formation of $CePO_4$, although it alone could account for the dramatic depletion in catalytic properties. It must be noticed that Ce is detected by EDS in the outermost layer of the washcoat, where a Ca- and P-rich crust is developed. Therefore, Ce phosphate can be also present in the outermost layer of washcoat what gives additional relevance to the formation of $CePO_4$. However, on the other hand the presence of CeO_2 islands can be possible in this real used TWC. This phase inhomogeinity can be due to a phase separation taking place during real ageing conditions or because a not very sophisticated and not optimal synthesis procedure was used in the preparation of this commercial TWC. They can interact faster with P than $Ce_{1-x}Zr_xO_2$ mixed oxide giving less importance to the detection of $CePO_4$ in the deterioration of the OSC properties.

Pb has been also demonstrated to poison the active metal sites by formation of a PGM–Pb alloy that displays considerable worse catalytic performance in eliminating NO, CO and unburned hydrocarbons than unpoisoned catalysts [15,18,44]. The formation of an impervious glassy Zn phosphate and an amorphous glaze-like Ca phosphate has been described also to participate in the deactivation of the catalyst because of the physical blockage of the active sites [16,17]. The explanation of how and the estimation of how deep a given contaminant is poisoning or affecting the catalytic properties needs additional research, basically conducted on model catalysts and on catalyst specifically contaminated ad hoc. Further research is being carried out in our laboratory in an attempt to gain more information on these aspects.

5. Conclusions

Catalytic properties of a real used TWC with ca. 30 000 km in which P, Ca, Zn, Pb, Cr, Ni, Fe, Cd and Cu deposition was detected by TXRF analysis were deteriorated. SEM-EDS studies showed that Ca and P were the main contaminating elements in the outermost layer of the washcoat. $CePO_4$ was detected by XRD in the used catalysts. TPO–TPR cycles showed that the Ce^{4+}/Ce^{3+} redox pair is locked. It is hypothesised that this must have deep implications on the needed OSC properties for the correct functioning of real TWC. The fact that Ce is detected by EDS in the outermost layer of the washcoat, where a Ca- and P-rich crust is developed and therefore that Ce phosphate can also be present there, provides additional importance to the hypothesis that the formation of $CePO_4$ could be involved in the damage of the catalytic properties.

Acknowledgements

References

[1] M. Shelef, R.W. McCabe, Catal. Today 62 (2000) 35.
[2] R.J. Farrauto, R.M. Heck, Catal. Today 51 (1999) 351.
[3] R.M. Heck, R.J. Farrauto, Appl. Catal. A: Gen. 221 (1/2) (2001) 443.
[4] A. Martinez-Arias, M. Fernandez-Garcia, A.B. Hungria, A. Iglesias-Juez, K. Duncan, R. Smith, J.A. Anderson, J.C. Conesa, J. Soria, J. Catal. 204 (1) (2001) 238.
[5] D.E. Angove, N.W. Cant, Catal. Today 63 (2000) 371.
[6] D.D. Beck, J.W. Sommers, C.L. DiMaggio, Appl. Catal. B 11 (3/4) (1997) 257.
[7] J.R. Gonzalez-Velasco, J.A. Botas, R. Ferret, M.P. Gonzalez-Marcos, J.L. Marc, M.A. Gutierrez-Ortiz, Catal. Today 59 (3/4) (2000) 395.
[8] F. Maire, M. Capelle, G. Meunier, J.F. Beziau, D. Bazin, H. Dexpert, F. Garin, J.L. Schmitt, G. Maire, Stud. Surf. Sci.

Catal. 96 (1995) 749 (Catalysis and Automotive Pollution Control III).

 [9] T.J. Truex, SAE Technical Paper Series (1999) 119769.

[10] C.H. Bartholomew, Appl. Catal. A: Gen. 212 (1/2) (2001) 17.

[11] P. Greening, Topics Catal. 16 (1–4) (2001) 5.

[12] L.A. Carol, N.E. Newman, G.S. Mann, SAE Technical Paper Series (1989) 892040.

[13] G. Colon, M. Pijolat, F. Valdivieso, H. Vidal, J. Kaspar, E. Finocchio, M. Daturi, C. Binet, J.C. Lavalley, R.T. Baker, S. Bernal, J. Chem. Soc., Faraday Trans. 94 (24) (1998) 3717.

[14] M.H. Yao, R.J. Baird, F.W. Kunz, T.E. Hoost, J. Catal. 166 (1) (1997) 67.

[15] M. Shelef, K. Otto, N.C. Otto, Adv. Catal. 27 (1978) 311.

[16] M.J. Rokosz, A.E. Chen, C.K. Lowe-Ma, A.V. Kucherov, D. Benson, M.C.P. Peck, R.W. McCabe, Appl. Catal. B: Environ. 33 (3) (2001) 205.

[17] D.R. Liu, J.S. Park, Appl. Catal. B: Environ. 2 (1) (1993) 49.

[18] W.B. Williamson, J. Perry, H.S. Gandhi, J.L. Bomback, Appl. Catal. 15 (1985) 277.

[19] T.N. Angelidis, S.A. Sklavounos, Appl. Catal. A 133 (1) (1995) 121.

[20] Fuels and Engines, Technology, Energy, Environment, J.C. Guibet. Editions Technip. Paris (1999).

[21] R. Fernández-Ruiz, J.P. Cabañero, E. Hernández, M. León, Analyst 126 (2001) 1797.

[22] R. Fernández-Ruiz, J. Capmany, J. Anal. Atom. Spectrom. 16 (2001) 867.

[23] R. Fernández-Ruiz, M. García-Heras, J.D. Tornero, J. Archaeol. Sci. 24 (1997) 1003.

[24] P. Malet, A. Caballero, J. Chem. Soc., Faraday Trans. 84 (7) (1988) 2369.

[25] E.S.J. Lox, B.H. Engler, in: G. Ertl, H. Knözinger, J. Weitkamp (Eds.), Environmental Catalysis—Mobile Sources, Wiley-VCH, New York, 1999, p. 1.

[26] T.N. Angelidis, V.G. Papadakis, Appl. Catal. B: Environ. 12 (1997) 193.

[27] H.S. Gandhi, W.B. Williamson, J.L. Bomback, Appl. Catal. 3 (1982) 79.

[28] J.I. Goldstein, D.E. Newbury, P. Echlin, D.C. Joy, C. Fiori, E. Lifshin, Scanning Electron Microscopy and X-ray Microanalysis, Plenum Press, New York, 1981.

[29] B. Angelé, K. Kirchner, Chem. Eng. Sci. 35 (1980) 2101.

[30] J. Kaspar, P. Fornasiero, M. Graziani, Catal. Today 50 (2) (1999) 285.

[31] B. Angelé, K. Kirchner, Chem. Eng. Sci. 35 (1980) 2089.

[32] P. Fornasiero, G. Balducci, R. Di Monte, J. Kaspar, V. Sergo, G. Gubitosa, A. Ferrero, M. Graziani, J. Catal. 164 (1) (1996) 173.

[33] P. Fornasiero, J. Kaspar, V. Sergo, M. Graziani, J. Catal. 182 (1) (1999) 56.

[34] P. Fornasiero, J. Kaspar, M. Graziani, J. Catal. 167 (2) (1997) 576.

[35] J.M. Gatica, R.T. Baker, P. Fornasiero, S. Bernal, J. Kaspar, J. Phys. Chem. B 105 (6) (2001) 1191.

[36] N. Hickey, P. Fornasiero, J. Kaspar, J.M. Gatica, S. Bernal, J. Catal. 200 (2001) 181.

[37] F.M.Z. Zotin, L. Tournayan, J. Varloud, V. Perrichon, R. Frety, Appl. Catal. A 98 (1) (1993) 99.

[38] G. Smedler, S. Eriksson, M. Lindblad, H. Bernler, S. Lundgren, E. Jobson, SAE Technical Paper Series (1993) 930944.

[39] P. Lucena, J.M. Vadillo, J. Laserna, Appl. Spectrosc. 55 (3) (2001) 267.

[40] P. Lucena, J.M. Vadillo, J.J. Laserna, Anal. Chem. 71 (1999) 4385.

[41] M. Tsuhako, M. Danjo, Y. Baba, M. Murakami, H. Nariai, I. Motooka, Bull. Chem. Soc. Jpn. 70 (1) (1997) 143.

[42] M. Tsuhako, S. Ikeuchi, T. Matsuo, I. Mutooka, M. Kobayashi, Bull. Chem. Soc. Jpn. 52 (4) (1975) 1034.

[43] R.G. Herman, A. Clearfield, J. Inorg. Nucl. Chem. 37 (1975) 1697.

[44] J. Goetz, M.A. Volpe, A.M. Sica, C.E. Gigola, R. Touroude, J. Catal. 167 (2) (1997) 314.